Particulate biogenic barium tracer of mesopelagic carbon remineralization in the Mediterranean Sea (PEACETIME project)

Stéphanie H.M. Jacquet[1*], Christian Tamburini[1], Marc Garel[1], Aurélie Dufour[1], France VanVambeke[1], Frédéric A.C. Le Moigne[1], Nagib Bhairy[1], Sophie Guasco[1]

[1]Aix Marseille Université, CNRS/INSU, Université de Toulon, IRD, Mediterranean Institute of Oceanography (MIO), UM 110, 13288 Marseille, France

[*]Correspondence to: S. Jacquet (*stephanie.jacquet@mio.osupytheas.fr)*

PEACETIME special issue

ABSTRACT

We report on the sub-basins variability of particulate organic carbon (POC) remineralization in the western and central Mediterranean Sea during a late spring period (PEACETIME cruise). POC remineralization rates were estimated using the excess biogenic particulate barium (Ba_{xs}) inventories in mesopelagic waters (100-1000 m) and compared with prokaryotic heterotrophic production (PHP). Ba_{xs}-based mesopelagic remineralization rates (MR) range from 25 ± 2 to 306 ± 70 mg C m^{-2} d^{-1}. MR are larger in the Alger (ALG) basin compared to the Tyrrhenian (TYR) and Ionian (ION) basins. Our Ba_{xs} inventories and integrated PHP data also indicates that significant mesopelagic remineralization occurs down to 1000 m depth in the ALG basin in contrast to the ION and TYR basins where remineralization is mainly located in the upper 500 m horizon. We proposed that the larger and deeper MR rates in the ALG basin would be sustained by an additional particles export event driven by deep convection. The TYR basin (in contrast to the ALG and ION basins) presents the impact of a previous dust event as reflected by our particulate Al water column concentrations. The ION and TYR basins are also the site of small-scale heterogeneity of stages of remineralization processes, as especially reflected by our Ba_{xs} inventories and integrated PHP data at the #Tyrr long duration station. This heterogeneity is linked to the mosaic of blooming and non-blooming patches reported in this area during the cruise. Contrastingly to the western Mediterranean Sea (ALG basin), the central Mediterranean Sea (ION and TYR basins) shows lower (intensity) and upper mesopelagic-layer restricted remineralization processes during the late spring PEACETIME cruise.

1. Introduction

In the ocean, remineralization rate associated with sinking particles is a crucial variable for air sea CO_2 balance [Kwon et al., 2009]. Most of the sinking particulate organic carbon (POC) conversion (i.e. remineralization) into CO_2 by heterotrophic organisms (i.e. respiration) occurs within the mesopelagic zone (100-1000 m) [Martin et al., 1987; Buesseler et al., 2007; Buesseler and Boyd, 2009]. A quantitative representation of this process is thus crucial to future predictions of the ocean's role in the global C cycle [IPCC, 2014]. Particulate biogenic barium (Ba_{xs}) is a geochemical tracer of POC remineralization in the mesopelagic layer. Ba_{xs} occurs in the form of barite ($BaSO_4$ crystals) in the dark ocean as a byproduct of prokaryotic remineralization. In a global ocean undersaturated with respect to barite [Monnin and Cividini, 2006], Ba_{xs} precipitates inside oversaturated biogenic micro-environments during POC degradation by heterotrophic prokaryotes, through sulfate and/or barium enrichment [Dehairs et al., 1980; Stroobant et al., 1991; Bertram and Cowen, 1997; Ganeshram et al., 2003]. By applying a transfer function relating Ba_{xs} to O_2 consumption [Dehairs et al., 1997] Ba_{xs} has been widely used since the 90's as an estimator of mesopelagic POC remineralization rates in various sectors of the Southern Ocean, North Pacific and North Atlantic [Cardinal et al., 2001, 2005; Dehairs et al., 2008; Jacquet et al., 2008a, 2008b, 2011, 2015; Planchon et al., 2013; Lemaitre et al., 2018]. Jacquet et al. [2021] recently reported that such transfer function could be applied in the Mediterranean Sea without restriction. This last study complemented previous investigations aiming at improving the use of Ba_{xs} to estimate local processes of POC remineralization in the Mediterranean Sea [Jacquet et al., 2016; Jullion et al., 2017]. The Mediterranean Sea represents a unique case study, mainly due to unresolved issues related to the imbalance in the regional C budget such as the coupling between surface biology and deeper remineralization, timescales of their variability between basins and discrepancies between mesopelagic trophic structure and respiration dynamics

[Sternberg et al., 2007, 2008; Santinelli et al., 2010; Lopez-Sandoval et al., 2011; Luna et al., 2012; Tanhua et al., 2013b; Malanotte-Rissoli et al., 2014].

The present work is part of the PEACETIME project (ProcEss studies at the Air-sEa Interface after dust deposition in the MEditerranean sea) (http://peacetime-project.org/). It aimed at studying the impact of atmospheric Saharan dust on the Mediterranean biogeochemistry [Guieu et al., 2020a]. Dust deposition is a major source of macro and micro nutrients and ballasted material to surface waters that likely impacts the biological carbon pump through organic matter production (i.e. primary production) and its subsequent export and remineralization in the water column [Pabortsava et al., 2017; Gazeau et al., 2021]. Overall, the aims of the present contribution to the PEACTIME project were: (1) to document particulate biogenic Ba_{xs} in different ecoregions of the western and central parts of the Mediterranean Sea. Previous Ba_{xs} data in the Mediterranean Sea are relatively scarce with limited vertical sampling resolution [Sanchez-Vidal et al., 2005] or restricted locations [Dehairs et al., 1987; Sternberg et al., 2007, 2008; van Beek et al., 2009]; (2) to determine the relationship between Ba_{xs} and environmental variability, including dust deposition, (3) to estimate Ba_{xs}-based POC remineralization rates (MR) at mesopelagic depths using the Dehairs' transfer function [Dehairs et al., 1997] which we have recently validated for the Mediterranean Sea [Jacquet et al., 2021], and (4) assess potential differences in remineralization length scale of POC in the various ecoregions of the Mediterranean Sea.

2. Material and methods

2.1 Study area

The PEACETIME cruise (https://doi.org/10.17600/17000300) was conducted during late spring from May 10 to June 11, 2017 (French R/V Pourquoi pas?) in the western and central Mediterranean (Figure 1a). The Mediterranean Sea is a semi-landlocked sea, with limited but

crucial exchange with the Atlantic Ocean, two deep overturning cells, one shallow circulation and a complex upper layer circulation with several permanent and quasi-permanent eddies.

The hydrography during the PEACETIME cruise was characterized by three-layers: surface, intermediate and deep waters, typical for the Mediterranean [Tamburini et al., 2013; Tanhua et al., 2013a; Hainbucher et al., 2014, Malanotte-Rizzoli et al., 2014]. Briefly, the main water masses are (see potential temperature – salinity diagram in Figure 1b): (1) from west to east surface Atlantic Water (SW) is gradually replaced by Ionian surface Water (ISW) and Levantine Surface water (LSW); (2) Winter Intermediate Water (WIW) and Levantine Intermediate water (LIW). LIW is present at intermediate depths (from 200 to 800 m) and is characterized by a local maximum of salinity and a local minimum of dissolved oxygen concentration; (4) Mediterranean Deep Water (MDW).

Three main ecoregions [Reygondeau et al., 2017; Ayata et al., 2018] were crossed during the cruise: the Algero-Provençal basin (later referred to as ALG), the Tyrrhenian basin (TYR) and the Ionian basin (ION) (Figure 1a). These basins displayed the typical eastward oligotrophic gradient as reported in previous studies [Moutin and Raimbault, 2002; Durrieu de madron et al., 2011; Pujo-Pay et al., 2011; Tanhua et al., 2013a; Reygondeau et al., 2017; Guieu et al., 2020a]. However, this trend was not homogeneous, as for instance in the Ionian Sea (a crossroad of waters of contrasted biological history) where a mosaic of blooming and non-blooming areas co-occured in spring [Berline et al., 2021]. A diatom-dominated deep chlorophyll maximum that coincided with a maximum in biomass and primary production (PP) was well developed and observed all along the cruise track (Marañón et al., 2021). PP is described in details in Van Wambeke et al. (this issue). Furthermore, important dust deposition affected the TYR basin a few days before our arrival at stations #Tyrr and #5, while in the ALG basin, dust deposition occurred few hours before our sampling at station

#Fast (Bressac et al., this issue). POC downward fluxes measured at 200 m depth were similar at the 3 long stations (#Fast, #Tyrr and #Ion).

2.2 Barium sampling and sample processing

Thirteen stations were sampled for particulate barium from the surface to 2000 m (thirty depths in total) in the ALG (stations #1, #2, #3, #10, #Fast, #9 and #4), TYR (stations #5, Tyrr and #6) and ION (stations #8, #7 and #Ion) basins (Table 1). Three of these stations were sampled twice on different days (long duration stations #Fast, #Tyrr and #Ion), but due to technical problem no particulate barium data are available for the second visit at station #Ion. Three days separate both visits at station #Fast and two days at #Tyrr.

For particulate barium, 4 to 6 L of seawater sampled using Niskin bottles were filtered onto 47 mm polycarbonate membranes (0.4 µm porosity) under slight overpressure supplied by filtered air. Filters were rinsed with a few mL of MQ grade water to remove sea salt, dried (50°C) and stored in Petri dishes for later analysis. In the laboratory, we performed a total digestion of filters using a concentrated tri-acid (0.5 mL HF /1.5 mL HNO_3 / HCl 1 mL; all Optima grade) mixture in closed teflon beakers overnight at 95°C in a clean pressurized room. After evaporation close to dryness, samples were re-dissolved into 10 mL of 2% HNO_3. Subsequently, samples were analysed for Ba and other elements of interest (i.e. Al, Na, Sr and Ca) by HR-ICP-MS (High Resolution-Inductively Coupled Plasma- Mass Spectrometry; ELEMENT XR, Thermo). Based on analyses of external certified reference standards, accuracy and reproducibility were both within ±5%. More details on sample processing and analysis are given in Cardinal et al. [2001] and Jacquet et al. [2015]. The presence of sea-salt was checked by analysing Na and the sea-salt particulate Ba contribution was found to be negligible (<0.1% of total Ba). Particulate biogenic barium in excess (hereafter referred to as Ba_{xs}) was calculated as the difference between total Ba and lithogenic Ba. The lithogenic Ba

concentration was determined using Al concentration and the upper continental crust (UCC) Ba:Al molar ratio [Dymond et al., 1992; Taylor and Mc Lennan, 1985]. The standard uncertainty [Ellison et al., 2000] on Ba_{xs} concentration ranges between 5.0 and 5.5%. The term "in excess" is used to indicate that concentrations are larger than the Ba_{xs} background (Ba BKG). The background (or residual value) is considered as "preformed" Ba_{xs} at zero oxygen consumption left over after transfer and partial dissolution of Ba_{xs} produced during degradation of previous particles export events. This background Ba_{xs} value likely depends on the saturation state of the water with respect to barite ($BaSO_4$, the main phase of particulate biogenic barium). Saturation indexes were reported in Jacquet et al. [2016] over a high resolution and quasi-zonal Mediterranean transect (M84/3 cruise; Tanhua et al., 2013a, 2013b). They revealed that the water column throughout the study area is largely undersaturated, with saturation state ranging between 0.2 and 0.6. A background Ba_{xs} value of 130 pM was recently reported in Jacquet et al. [2021]. It is close to the average Ba_{xs} contents observed at greater depth (>1000 m) in the present study (see below).

2.3 Prokaryotic heterotrophic production

Prokaryotic heterotrophic production (PHP) estimation was measured by the L-[4,5-3H]-Leucine (^{3}H-Leu, specific activity 109 Ci mmol^{-1}, PerkinElmer®) incorporation technique (Kirchman, 1993). Details of the protocols can be found in Van Wambeke et al. (2021). Briefly, in epipelagic layers (0-200 m) 1.5 ml seawater samples were incubated at 20 nM ^{3}H-Leu final concentration using the microcentrifuge technique (Smith and Azam, 1992). For the mesopelagic layers, 20 ml (200-800 m depth) and 40 ml (below 800 m depth) seawater samples were incubated using 20 nM and 10 nM ^{3}H-Leu final concentration, respectively, using the filtration technique (Tamburini et al., 2002). Samples were incubated at in situ temperature. To calculate PHP, we used the empirical conversion factor of 1.5 ng C per pmol

of incorporated leucine assuming that isotopic dilution was negligible under saturating concentrations of leucine as checked occasionally from concentration kinetics (Van Wambeke et al., 2021).

2.4 POC remineralization rates

We recently reported on the validity of the Dehairs's transfer function [Dehairs et al., 1997] in the Mediterranean basin to estimate mesopelagic POC remineralization [Jacquet et al., 2021]. We applied the similar approach to estimate remineralization rates (MR):

$$MR = [(Ba_{xs} - Ba\ BKG)/17450] \times Z \times RR \quad (Eq.1)$$

where Ba_{xs} is the depth-weighted average Ba_{xs} concentration (DWA; pM), i.e. the Ba_{xs} inventory divided by the depth layer considered Z, and RR the Redfield C/O_2 molar ratio (127/175; Broecker et al., 1985). As reported above, a Ba BKG concentration of 130 pM was used. MR rates were then integrated over the 100-500 m (upper mesopelagic zone) and 100-1000 m (entire mesopelagic zone) depth layers.

3. Results

Particulate biogenic Ba_{xs}, biogenic Ba fraction (%) and particulate Al, Sr and Ca concentrations are reported in Figure 2 in the upper 2000 m of the water column along a zonal transect crossing the three main sub-basins. PHP rates are also reported in Figure 2 in the upper 500 m along the same transect.

Ba_{xs} displayed a similar water column distribution as reported in various sectors of the global Ocean, i.e. relatively low surface concentrations, a maximum in the mesopelagic layer (100-1000 m) followed by a decrease of concentrations back to a background level at deeper depths, usually 1000 m (Figure 3). At stations #9, #Tyrr, #8 and #Ion, Ba_{xs} concentrations in the upper 100 m were quite high (>5000 pM), with values reaching up to 11700 pM at 80 m

depth at station #Tyrr (Figure 2a). Such high Ba_{xs} concentrations in the upper layers are quite unusual, though similar values (up to 9000 pM) were occasionally observed in earlier Southern Ocean studies [Dehairs et al., 1991, 1997; Jacquet et al., 2007b, 2008a, 2008b]. The high Ba_{xs} values at stations #Tyrr and #Ion were associated with higher Sr (up to 4267 pM at 100 m at station #Ion) and Ca (>130 nM) concentrations (Figure 2d, e). Thoughtout the water column, Sr and Ca concentrations ranged from to 448 to 6938 pM and from 30 to 488 nM, respectively. Sr/Ca molar ratios ranged from 7 to 45 mmol mol^{-1}whithin the range of ratios reported in organic material [Martin and Knauer, 1976]. The upper mesopelagic layer (100-500 m) showed the characteristic Ba excess (maximum), as illustrated in Figure 3a. The lithogenic impact on the Ba_{xs} signal was relatively low (<20 %) except at stations #4, #5 and #Tyrr where it reached up to 30 % at some depths in the water column (Figures 2b, 3b). High Ba_{xs} concentrations at stations in the ALG basin and at station #7 in the ION basin extended deeper than at stations in the TYR basin (Figure 2a). At station #Ion Ba_{xs} maximum coincided with higher Ca (up to 186 nM) concentrations in the upper mesopelagic layer (Figure 2e). However, the Ba_{xs} maximum also extented deeper. This is especially salient at stations in the ALG basin. At the other stations Ba_{xs} concentrations below 500 m decreased to reach the background value of around 130 pM. Among stations sampled twice for barium during the cruise, station #Fast (ALG basin) presented similar Ba_{xs} profiles except between 400 and 1000 m depth where lower concentrations were measured during the second visit (3 days later; Figure 3a). The Ba_{xs} signal was mostly biogenic and rather stable over the whole water column at this station. This was also the case at station #Ion. In contrast, at station #Tyrr differences between Ba_{xs} profiles mainly occurred in the surface layer and upper mesopelagic layer, with relatively higher Ba_{xs} peaks during the second visit (2 days later; Figure 3b). The biogenic Ba fraction was also more variable throughout the water column at #Tyrr.

PHP rates decreased from west to east in surface waters (Figure 2f). At station #Fast,

PHP rates decreased from 49 ng C l^{-1} h^{-1} in surface to values between 7 and 11 ng C l^{-1} h^{-1} at 100 m depth and below 6 ng C l^{-1} h^{-1} below 200 m depth (Figure 3d). Same trends were found at #Tyrr and #Ion with values in surface waters around 36 and 25 ng C l^{-1} h^{-1} respectively (Figures 3e and 3f).

Depth-weighted average (DWA) concentrations of Ba_{xs} are reported in Table 1 and Figure 5 for the upper (100-500 m) and entire (100-1000 m) mesopelagic layer. Since the base of the mixed layer was shallower than 100 m, this depth is taken as the upper boundary of the mesopelagic domain. DWA values ranged from 221 to 979 pM. On average, stations located in the ALG basin presented higher DWA than in the TYR and ION basins. DWA Ba_{xs} values remained rather stable over the 3–day period at station #Fast between 100 and 500 m depth, but decreased in deeper layers (Figure 5). As a consequence, the DWA changed from 527 to 381 pM for the entire 100-1000 depth layer. In contrast, at station #Tyrr DWA Ba_{xs} values for the 100-500 m and 100-1000 m depth layers increased over the 2–day period (from 284 to 542 pM and from 200 to 380 pM, respectively). On average DWA Ba_{xs} reached 577±286, 378±123 and 529±213 pM (100-500 m), and 527±288, 280±82 and 358±112 pM (100-1000 m) in the ALG, TYR and ION basin, respectively.

4. Discussion

4.1 Ba_{xs} distributions across the sub-basins

The very high Ba_{xs} concentrations reported in the surface layer at stations #9, #Tyrr, #8 and #Ion were associated with local Sr and Ca maxima, likely linked to potentially ballasted phytoplankton-derived material. Similar observations were previously reported in the Southern Ocean, revealing that in the surface water particulate Ba_{xs} is incorporated into or adsorbed onto biogenic material, with barite being a minor component [Dehairs et al., 1991, 1997; Jacquet et al., 2007a, 2008a, 2008b]. In deeper layers, Ba_{xs} presented the characteristic

maximum reflecting mesopelagic remineralization processes. Mesopelagic Ba_{xs} distributions presented here were similar to those reported in Jacquet et al. [2021] and Sternberg et al. [2008] in the northwestern Mediterranean Sea (ANTARES and DYFAMED observatory sites, respectively). The Ba_{xs} maximum extended down to 1000 m depth in the ALG basin, while it was mostly located in the upper 500 m depth in the TYR basin. The lithogenic impact on the Ba_{xs} signal was relatively very low (<5%), except at stations #4, #5 and #Tyrr where it was more variable and reached up to 30 % at some depths (Figure 2b and 2c). A large dust deposition event occurred over a large area including the southern Tyrrhenian Sea just before the beginning of the PEACETIME campaign. Particulate Al concentrations and estimated lithogenic Ba fraction were sampled at these stations 5 to 12 days after the event and reflected the impact of this dust event in depth. These conclusions are further supported by results reported in Bressac et al. [this issue], showing that Saharan dust depositions strongly impacted Stations #4, #5, #Tyrr and #6 whereby a significant fraction of dust particles was transferred to mesopelagic depths.

4.2 Mesopelagic Ba_{xs} and prokaryotic heterotrophic production

Previous studies highlighted the relationship between the mesopelagic Ba_{xs} and the vertical distribution of prokaryotic heterotrophic production (PHP), reflecting the temporal progression of POC remineralization processes. In mesopelagic layers, Ba_{xs} content is smaller when most of the PHP occurs in the upper mixed layer (indicating an efficient, close to complete remineralization within the surface), compared to situations where a significant part of PHP is located deeper in the water column (reflecting significant deep prokaryotic activity and POC export). Figure 3 shows the PHP profiles at long station #Fast, #Tyrr and #Ion (see also VanWambeke et al. [2021] for more detail on PHP). Figure 4 shows the ratio of integrated surface (100 m) to integrated upper mesopelagic (500 m) PHP vs. DWA Ba_{xs}

262 calculated over the 100-500 m depth interval. Results are confronted to the data obtained in
263 the Southern Ocean [Jacquet et al., 2008a, 20015] and recently in the northeast Atlantic and
264 northwestern Mediterranean Sea (PAP and ANTARES observatory sites, respectively)
265 [Jacquet et al., 2021]. The blue line in Figure 4 represents the trend obtained during KEOPS2
266 [Jacquet et al., 2015]; it does not include encircled data points referred to as "season
267 advancement". Results during PEACETIME followed a similar trend than found for KEOPS2
268 with higher DWA Ba_{xs} in situation where a significant part of column-integrated PHP is
269 located deeper in the water column (high Int.PHP100/Int.PHP500 ratio, Figure 4). Note that
270 some data points, characterized by low DWA Ba_{xs} values, did not follow the trend from
271 KEOPS2 (stations #3, #5 and #Tyrr2). During KEOPS2, the lowest DWA were reported for
272 stations located in a meander and reflecting different (earlier) stages of a bloom compared to
273 the other stations (see "season advancement" in Figure 4). Similarly, station #5 and #Tyrr2
274 reflected the temporal evolution of the establishment (or advanced stages) of mesopelagic
275 remineralization processes in the TYR basin compared to the other basins. Measurements
276 carried out during the second visit at station #Tyrr two days later corroborated this hypothesis
277 showing an increase in remineralization in the upper mesopelagic layer (DWV Ba_{xs} increased
278 from 284 to 542 pM). At the DYFAMED station, Sternberg et al. [2008] reported the seasonal
279 evolution of Ba_{xs} profiles on a monthly basis between February and June 2003. These authors
280 showed the mesopelagic Ba_{xs} build up (and barite stock increase) following the spring
281 phytoplankton bloom development, enhanced POC fluxes and subsequent remineralization.
282 Overall, DWA Ba_{xs} reported in the present study were higher than those reported by
283 Sternberg et al. [2008] (maximum of 463 pM; 0-600 m). The variability over the two days
284 period at station #Tyrr was of the same order of magnitude as the seasonal DWA Ba_{xs}
285 dynamics found at DYFAMED and similar to changes found over a few days to week period
286 in different sectors of the Southern Ocean [Cardinal et al., 2005; Jacquet et al., 2007a; 2015].

The column-integrated PHP vs. DWA Ba_{xs} ratio at station #Tyrr confirms that the second occupation experienced higher remineralization rates in the upper mesopelagic layer than during the first one (Table 1).

4.3 Mesopelagic C remineralization

POC remineralization rates (MR) estimated from DWA Ba_{xs} values using Eq. (1) are shown in Figure 5 for the upper (100-500 m) and entire (100-1000 m) mesopelagic layer together with primary productivity [van Wambecke et al., 2021]. MR ranged from 25 ± 2 to 306 ± 70 mg C m^{-2} d^{-1} and primary production ranged from 138 to 284 mg C m^{-2} d^{-1}. Large difference in MR between the upper and the whole mesopelagic layers can be seen in the ALG basin. This is more pronounced at station #9 with MR of 91 mg C m^{-2} d^{-1} in the upper (100 to 500 m depth) layer and 306 mg C m^{-2} d^{-1} in the entire mesopelagic layer (Figure 5). These results show that significant remineralization occurred between 500 and 1000 m in the ALG basin in contrast to the ION and TYR basins where remineralization occurred mainly in the mesopelagic layer between 100 and 500 m depth. Similar conclusion was reached by Jullion et al. [2017] from dissolved Ba and Parametric Optimum Multiparameter (POMP)-derived POC remineralization rates along a zonal transect between the Lebanon coast and Gibraltar (from 156 to 348 mg C m^{-2} d^{-1}; M84/3 cruise, April 2011). Independent of any dust input considerations, Jullion et al. [2017] showed significant differences in the mesopelagic MR between the western and eastern Mediterranean, indicating an additional organic carbon export pathway to depth. The western basin is indeed the site of deep shelf and open ocean convection, transferring organic matter to deeper layers [Durrieu de Madron et al., 2013; Stabholz et al., 2013]. The larger MR fluxes found in the ALG basin during PEACETIME are in line with an ecoregion with recurrent injection of material by winter convection (hypothesis of particle injection pump; Boyd et al. [2019]), sustaining higher rates of remineralization

below 500 m depth. In contrast in the TYR basin remineralization was mainly located in the upper mesopelagic layer. Stations in the TYR basin received dust inputs a few days before our arrival at these stations; the particulate Al concentrations and estimated lithogenic Ba fraction reflected the impact of this event (Figure 2; Bressac et al., this issue). At station #Tyrr the DAW Ba_{xs} vs. column-integrated PHP increase between the two visits indicated higher MR rates. MR were mainly localized in the upper 500 m. Another atmospheric deposition event occurred on June 5, a few hours after the first sampling at station #Fast in the ALG basin. However, station #Fast does not present any evidence of an impact at mesopelagic depths on particulate Al concentrations and estimated lithogenic Ba. In contrast to conditions in the surface mixed layer, the generation of an observable signal from the mesopelagic remineralization and subsequent Ba_{xs} formation to a single dust event would require more time than the time span between atmospheric deposition and sampling at #Fast (in contrast to station #Tyrr where the dust event occurred 5 to 12 days before). In the ION basin where stations did not reflect the impact of any deposition event and were not subject to potential deep convection, DWA Ba_{xs} and MR fluxes were mostly restricted to the upper mesopelagic layer. Berline et al. [this issue] report small-scale heterogeneity of particles abundances at ION stations, emphasizing the spatial decoupling between particle production and particle distribution and adding complexity in estimating the time lag between production and export of particles, and thus C transfer eat depth [Stange et al., 2017; Henson et al., 2011]. Further, no significant surface production event occurred in the ION basin However, surface particles at station #8 seemed related to a past production event without significant vertical export by the time the station was sampled. As reported in Van Wambeke et al. [this issue], primary production fluxes were slightly higher in the ION basin (from 158 to 208 mg C m^{-2} d^{-1}) than in the TYR basin (from 142 to 170 mg C m^{-2} d^{-1}). Overall, DWA Ba_{xs} and MR fluxes reported in the ION basin would thus reflect earlier stage of export and remineralization processes. The

same applies to station #Tyrr 2 (in contrast to #Tyrr4) according to the DWA Ba_{xs} vs integrated-PHP trend.

5. Conclusion

The present paper expands the data coverage of Ba_{xs} distribution in the ALG, TYR and ION basins (western and central Mediterranean Sea) in late spring 2017. Results highlight that mesopelagic remineralization processes are mainly located in the upper 500 m horizon in the TYR and ION basins, while they occur in the lower mesopelagic zone (down to 1000 m) in the ALG basin. We suggest that particle injection driven by the seasonal winter deep convection in the western basin would sustain the larger and deeper MR rates we observed in the ALG basin. At both TYR and ION basins, Ba_{xs} indicated lower (intensity) and upper mesopelagic-layer restricted remineralization processes that could be the results of a previous dust deposition event (in particular at #Tyrr) or the patchiness of time lags between production and export of particles.

Data availability

Underlying research data are being used by researcher participants of the PEACETIME campaign to prepare other papers, and therefore data are not publicly accessible at the time of publication. Data will be accessible once the special issue is completed (June 2021) (http://www.obs-vlfr.fr/proof/php/PEACETIME/peacetime.php; last access 02/04/2021). The policy of the database is detailed here: http://www.obs-vlfr.fr/proof/dataconvention.php and https://www.seanoe.org/data/00645/75747/ (last access 02/04/2021).

Author contributions

SJ wrote the manuscript with the contribution of all co-authors.

Competing interests

The authors declare that they have no known competing financial interests or personal relationships that could have appeared to influence the work reported in this paper.

Special issue statement

This article is part of the special issue “Atmospheric deposition in the low-nutrient–low-chlorophyll (LNLC) ocean: effects on marine life today and in the future (ACP/BG interjournal SI)”. It is not associated with a conference.

Acknowledgments

This study is a contribution to the PEACETIME project (http://peacetime-project.org), a joint initiative of the MERMEX and ChArMEx components supported by CNRS-INSU, IFREMER, CEA, and Météo-France as part of the programme MISTRALS coordinated by INSU. PEACETIME was endorsed as a process study by GEOTRACES. It is also a contribution to SOLAS and IMBER. We thank the captain and the crew of the RV Pourquoi Pas? for their professionalism and their work at sea. We warmly thank C. Guieu and K. Deboeufs, as coordinators of the program PEACETIME and chiefs scientists of the campaing. This work is a contribution to the "AT – POMPE BIOLOGIQUE" of the Mediterranean Institute of Oceanography (MIO). The instrument (ELEMENT XR, ThermoFisher) was supported in 2012 by European Regional Development Fund (ERDF).

Figures

Figure 1: (a) Map of the study area showing the three sub-basins (ALG, TYRR and ION) with stations' locations. The dashed line represents the zonal transect reported in Figure 2; (b) Potential temperature – salinity diagram with isopynals (kg m^{-3}) for PEACETIME profiles. Graph produced using Ocean Data View (Schlitzer, 2002).

Figure 2: Sections of (a) particulate biogenic Ba (Ba_{xs}, pM), (c) Al (pM), (d) Sr (pM) and (e) Ca (nM) concentrations, and (b) % biogenic Ba (Ba_{xs}) in the upper 2000 m water column. (f) Section of PHP (ngC L^{-1} h^{-1}) in the upper 500 m of the water column. Graph produced using Ocean Data View (Schlitzer, 2002).

Figure 3: (a-c) Ba_{xs} (pM) and (d-f) (ngC L^{-1} h^{-1}) profiles in the upper 2000 m and 1000 m of the water column, respectively, at long stations #Fast, #Tyrr and #Ion. (a-c) The dashed grey line represents the Ba_{xs} background (BKG) and the grey area represents the fraction for which Ba_{xs} is mostly biogenic.

Figure 4: Ratio of surface layer integrated PHP (Int.PHPx1) to mesopelagic integrated PHP (Int.PHPx2) versus mesopelagic depth-weighted average (DWA) Ba_{xs} (pM) during PEACETIME. The same data are reported for the KEOPS1 and KEOPS2 cruises (Southern Ocean; Jacquet et al., 2015) and at the PAP (NE-Atlantic) and ANTARES/EMSO-LO (NW-Mediterranean Sea) observatory sites (Jacquet et al., 2021). The blue line (R^2=0.88) represents the trend reported during KEOPS2 (Jacquet et al., 2005). The data points referred to as "season advancement" (encircle by the blue line) were excluded from the KEOPS2 regression analysis shown here.

Figure 5: integrated POC remineralization rates (mg C m^{-2} d^{-1}) in the upper (100 to 500 m depth) and entire (100 to1000 m depth) mesopelagic layer in the ALG, TYR and ION basins. Open squares represent primary production (mg C m^{-2} d^{-1}; Van Wambeke et al., this issue).

Tables

Table 1: Depth-weighted average (DWA) concentrations of Ba_{xs} (pM) and remineralization rates (MR; mg C m^{-2} d^{-1}) for the upper (100 to 500 m depth) and entire (100 to 1000 m depth) mesopelagic layer.

418 **References**

419 Ayata, S.-D., Irisson, J.-O., Aubert, A., Berline, L., Dutay, J.-C., Mayot, N., Nieblas, A.-E.,
420 D'Ortenzio, F., Palmiéri, J., Reygondeau, G., Rossi, V., and Guieu, C.: Regionalisation of the
421 Mediterranean basin, a MERMEX synthesis, Prog. Oceanogr., 163, 7–20,
422 https://doi.org/10.1016/j.pocean.2017.09.016, 2018.

423 van Beek, P., Sternberg, E., Reyss, J.-L., Souhaut, M., Robin, E., and Jeandel, C.:
424 228Ra/226Ra and 226Ra/Ba ratios in the Western Mediterranean Sea: Barite formation and
425 transport in the water column, Geochim. Cosmochim. Ac., 73, 4720–4737,
426 https://doi.org/10.1016/j.gca.2009.05.063, 2009.

427 Berline, L., Doglioli, A. M., Petrenko, A., Barrillon, S., Espinasse, B., Le Moigne, F. A. C.,
428 Simon-Bot, F., Thyssen, M., and Carlotti, F.: Long distance particle transport to the central
429 Ionian Sea, Biogeosciences, 2021, 1–28, https://doi.org/10.5194/bg-2020-481, 2021.

430 Bertram, M. and P. Cowen, J.: Morphological and compositional evidence for biotic
431 precipitation of marine barite, J. Mar. Res., 55, 577–593, 1997.

432 Boyd, P., Claustre, H., Levy, M., Siegel, D., and Weber, T.: Multi-faceted particle pumps
433 drive carbon sequestration in the ocean, Nature, 568, 327–335,
434 https://doi.org/10.1038/s41586-019-1098-2, 2019.

435 Broecker, W. S., Takahashi, T., and Takahashi, T.: Sources and flow patterns of deep-ocean
436 waters as deduced from potential temperature, salinity, and initial phosphate concentration, J.
437 Geophys. Res., 90, 6925–6939, https://doi.org/10.1029/JC090iC04p06925, 1985.

438 Buesseler, K. O. and Boyd, P. W.: Shedding light on processes that control particle export and
439 flux attenuation in the twilight zone of the open ocean, Limnol. Oceanogr., 54, 1210–1232,
440 https://doi.org/10.4319/lo.2009.54.4.1210, 2009.

441 Buesseler, K. O., Lamborg, C. H., Boyd, P. W., Lam, P. J., Trull, T. W., Bidigare, R. R.,
442 Bishop, J. K. B., Casciotti, K. L., Dehairs, F., Elskens, M., Honda, M., Karl, D. M., Siegel, D.

A., Silver, M. W., Steinberg, D. K., Valdes, J., Van Mooy, B., and Wilson, S.: Revisiting Carbon Flux Through the Ocean's Twilight Zone, Science, 316, 567–570, https://doi.org/10.1126/science.1137959, 2007.

Cardinal, D., Dehairs, F., Cattaldo, T., and André, L.: Geochemistry of suspended particles in the Subantarctic and Polar Frontal zones south of Australia: Constraints on export and advection processes, J. Geophys. Res., 106, 31637–31656, https://doi.org/10.1029/2000JC000251, 2001.

Cardinal, D., Savoye, N., Trull, T. W., André, L., Kopczynska, E. E., and Dehairs, F.: Variations of carbon remineralisation in the Southern Ocean illustrated by the Baxs proxy, Deep-Sea Res. Pt. I, 52, 355–370, https://doi.org/10.1016/j.dsr.2004.10.002, 2005.

Dehairs, F., Chesselet, R., and Jedwab, J.: Discrete suspended particles of barite and the barium cycle in the open ocean, Earth. Planet. Sc. Lett., 49, 528–550, https://doi.org/10.1016/0012-821X(80)90094-1, 1980.

Dehairs, F., Lambert, C. E., Chesselet, R., and Risler, N.: The biological production of marine suspended barite and the barium cycle in the Western Mediterranean Sea, Biogeochemistry, 4, 119–140, https://doi.org/10.1007/BF02180151, 1987.

Dehairs, F., Stroobants, N., and Goeyens, L.: Suspended barite as a tracer of biological activity in the Southern Ocean, Mar. Chem., 35, 399–410, http://dx.doi.org/10.1016/S0304-4203(09)90032-9, 1991.

Dehairs, F., Shopova, D., Ober, S., Veth, C., and Goeyens, L.: Particulate barium stocks and oxygen consumption in the Southern Ocean mesopelagic water column during spring and early summer: relationship with export production, Deep-Sea Res. Pt. II, 44, 497–516, https://doi.org/10.1016/S0967-0645(96)00072-0, 1997.

Dehairs, F., Jacquet, S., Savoye, N., Van Mooy, B. A. S., Buesseler, K. O., Bishop, J. K. B., Lamborg, C. H., Elskens, M., Baeyens, W., Boyd, P. W., Casciotti, K. L., and Monnin, C.:

468 Barium in twilight zone suspended matter as a potential proxy for particulate organic carbon
469 remineralization: Results for the North Pacific, Deep-Sea Res. Pt. II, 55, 1673–1683,
470 https://doi.org/10.1016/j.dsr2.2008.04.020, 2008.
471 Durrieu de Madron, X., Guieu, C., Sempéré, R., Conan, P., Cossa, D., D'Ortenzio, F.,
472 Estournel, C., Gazeau, F., Rabouille, C., Stemmann, L., Bonnet, S., Diaz, F., Koubbi, P.,
473 Radakovitch, O., Babin, M., Baklouti, M., Bancon-Montigny, C., Belviso, S., Bensoussan, N.,
474 Bonsang, B., Bouloubassi, I., Brunet, C., Cadiou, J.-F., Carlotti, F., Chami, M., Charmasson,
475 S., Charrière, B., Dachs, J., Doxaran, D., Dutay, J.-C., Elbaz-Poulichet, F., Eléaume, M.,
476 Eyrolles, F., Fernandez, C., Fowler, S., Francour, P., Gaertner, J. C., Galzin, R., Gasparini, S.,
477 Ghiglione, J.-F., Gonzalez, J.-L., Goyet, C., Guidi, L., Guizien, K., Heimbürger, L.-E.,
478 Jacquet, S. H. M., Jeffrey, W. H., Joux, F., Le Hir, P., Leblanc, K., Lefèvre, D., Lejeusne, C.,
479 Lemé, R., Loÿe-Pilot, M.-D., Mallet, M., Méjanelle, L., Mélin, F., Mellon, C., Mérigot, B.,
480 Merle, P.-L., Migon, C., Miller, W. L., Mortier, L., Mostajir, B., Mousseau, L., Moutin, T.,
481 Para, J., Pérez, T., Petrenko, A., Poggiale, J.-C., Prieur, L., Pujo-Pay, M., Pulido-Villena,
482 Raimbault, P., Rees, A. P., Ridame, C., Rontani, J.-F., Ruiz Pino, D., Sicre, M. A.,
483 Taillandier, V., Tamburini, C., Tanaka, T., Taupier-Letage, I., Tedetti, M., Testor, P.,
484 Thébault, H., Thouvenin, B., Touratier, F., Tronczynski, J., Ulses, C., Van Wambeke, F.,
485 Vantrepotte, V., Vaz, S., and Verney, R.: Marine ecosystems' responses to climatic and
486 anthropogenic forcings in the Mediterranean, Prog. Oceanogr., 91, 97–166,
487 https://doi.org/10.1016/j.pocean.2011.02.003, 2011.
488 Dymond, J. R., Suess, E., and Lyle, M.: Barium in deep-sea sediment: a geochemical proxy
489 for paleoproductivity, Paleoceanography, 7, 163–181, 1992.
490 Ellison, S. L. R.: Eurachem/CITAC Guide CG4, Quantifying Uncertainty in Analytical
491 Measurement, 2nd Edn., edited by: Ellison, S. L. R., Rosslein, M., and Williams, A., 120 pp.,
492 ISBN 0948926 15 5, 2000.

493 Ganeshram, R. S., François, R., Commeau, J., and Brown-Leger, S. L.: An experimental
494 investigation of barite formation in seawater, Geochim. Cosmochim. Ac., 67, 2599–2605,
495 https://doi.org/10.1016/S0016-7037(03)00164-9, 2003.
496 Gazeau, F., Van Wambeke, F., Marañon, E., Pérez-Lorenzo, M., Alliouane, S., Stolpe, C.,
497 Blasco, T., Leblond, N., Zäncker B., Engel A., Marie, B., Dinasquet, J., and Guieu C.: Impact
498 of dust addition on the metabolism of Mediterranean plankton communities and carbon export
499 under present and future conditions of pH and temperature, Biogeosciences Discuss.
500 [preprint], https://doi.org/10.5194/bg-2021-20, in review, 2021.
501 Guieu, C., D'Ortenzio, F., Dulac, F., Taillandier, V., Doglioli, A., Petrenko, A., Barrillon, S.,
502 Mallet, M., Nabat, P., and Desboeufs, K.: Introduction: Process studies at the air–sea interface
503 after atmospheric deposition in the Mediterranean Sea – objectives and strategy of the
504 PEACETIME oceanographic campaign (May–June 2017), Biogeosciences, 17, 5563–5585,
505 https://doi.org/10.5194/bg-17-5563-2020, 2020a.
506 Guieu, C., and Desboeufs, K. : PEACETIME cruise, RV Pourquoi pas?,
507 https://doi.org/10.17600/17000300, 2017.
508 Guieu, C., Desboeufs, K., Albani, S., et al.: Biogeochemical dataset collected during the
509 PEACETIME cruise, available at: https://www.seanoe.org/data/00645/75747/, 2020b.
510 Hainbucher, D., Rubino, A., Cardin, V., Tanhua, T., Schroeder, K., and Bensi, M.:
511 Hydrographic situation during cruise M84/3 and P414 (spring 2011) in the Mediterranean
512 Sea, Ocean Sci., 10, 669–682, https://doi.org/10.5194/os-10-669-2014, 2014.
513 Henson, S. A., Sanders, R., Madsen, E., Morris, P. J., Le Moigne, F., and Quartly, G. D.: A
514 reduced estimate of the strength of the ocean's biological carbon pump, Geophys. Res. Lett.,
515 38, L04606, https://doi.org/10.1029/2011GL046735, 2011.
516 IPCC: 5th Assessment Report (AR5) Climate Change 2013, Working Group 1, January 2014.

517 Jacquet, S. H. M., Dehairs, F., Elskens, M., Savoye, N., and Cardinal, D.: Barium cycling
518 along WOCE SR3 line in the Southern Ocean, Mar. Chem., 106, 33–45,
519 https://doi.org/10.1016/j.marchem.2006.06.007, 2007a.
520 Jacquet, S. H. M., Henjes, J., Dehairs, F., Worobiec, A., Savoye, N., and Cardinal, D.:
521 Particulate Ba-barite and acantharians in the Southern Ocean during the European Iron
522 Fertilization Experiment (EIFEX), J. Geophys. Res., 112,
523 https://doi.org/10.1029/2006JG000394, 2007b.
524 Jacquet, S. H. M., Savoye, N., Dehairs, F., Strass, V. H., and Cardinal, D.: Mesopelagic
525 carbon remineralization during the European Iron Fertilization Experiment, Global
526 Biogeochem. Cycles, 22, GB1023, https://doi.org/10.1029/2006GB002902, 2008a.
527 Jacquet, S. H. M., Dehairs, F., Savoye, N., Obernosterer, I., Christaki, U., Monnin, C., and
528 Cardinal, D.: Mesopelagic organic carbon remineralization in the Kerguelen Plateau region
529 tracked by biogenic particulate Ba, Deep-Sea Res. Pt. II, 55, 868–879,
530 https://doi.org/10.1016/j.dsr2.2007.12.038, 2008b.
531 Jacquet, S. H. M., Dehairs, F., Dumont, I., Becquevort, S., Cavagna, A.-J., and Cardinal, D.:
532 Twilight zone organic carbon remineralization in the Polar Front Zone and Subantarctic Zone
533 south of Tasmania, Deep-Sea Res. Pt. II, 58, 2222–2234,
534 https://doi.org/10.1016/j.dsr2.2011.05.029, 2011.
535 Jacquet, S. H. M., Dehairs, F., Lefèvre, D., Cavagna, A. J., Planchon, F., Christaki, U.,
536 Monin, L., André, L., Closset, I., and Cardinal, D.: Early spring mesopelagic carbon
537 remineralization and transfer efficiency in the naturally iron-fertilized Kerguelen area,
538 Biogeosciences, 12, 1713–1731, https://doi.org/10.5194/bg-12-1713-2015, 2015.
539 Jacquet, S. H. M., Monnin, C., Riou, V., Jullion, L., and Tanhua, T.: A high resolution and
540 quasi-zonal transect of dissolved Ba in the Mediterranean Sea, Mar. Chem., 178, 1–7,
541 https://doi.org/10.1016/j.marchem.2015.12.001, 2016.

Jacquet, S. H. M., Lefèvre, D., Tamburini, C., Garel, M., Le Moigne, F. A. C., Bhairy, N., and Guasco, S.: On the barium–oxygen consumption relationship in the Mediterranean Sea: implications for mesopelagic marine snow remineralization, Biogeosciences, 18, 2205–2212, https://doi.org/10.5194/bg-18-2205-2021, 2021.

Jullion, L., Jacquet, S. H. M., and Tanhua, T.: Untangling biogeochemical processes from the impact of ocean circulation: First insight on the Mediterranean dissolved barium dynamics, Global Biogeochem. Cycles, 31, 1256–1270, https://doi.org/10.1002/2016GB005489, 2017.

Kirchman, D. L.: Leucine incorporation as a measure of biomass production by heterotrophic bacteria, in: Handbooks of methods in aquatic microbial ecology,, edited by: Kemp, P. F., Sherr, B. F., Sherr, E. B., and Cole, J. J., Lewis Publishers, Boca Raton, Ann Arbor, London, Tokyo, 509–512, 1993.

Kwon, E. Y., Primeau, F., and Sarmiento, J. L.: The impact of remineralization depth on the air–sea carbon balance, Nat. Geosci., 2, 630–635, https://doi.org/10.1038/ngeo612, 2009.

Lemaitre, N., Planquette, H., Planchon, F., Sarthou, G., Jacquet, S., García-Ibáñez, M. I., Gourain, A., Cheize, M., Monin, L., André, L., Laha, P., Terryn, H., and Dehairs, F.: Particulate barium tracing of significant mesopelagic carbon remineralisation in the North Atlantic, Biogeosciences, 15, 2289–2307, https://doi.org/10.5194/bg-15-2289-2018, 2018.

López-Sandoval, D. C., Fernández, A., and Marañón, E.: Dissolved and particulate primary production along a longitudinal gradient in the Mediterranean Sea, Biogeosciences, 8, 815–825, https://doi.org/10.5194/bg-8-815-2011, 2011.

Luna, G. M., Bianchelli, S., Decembrini, F., De Domenico, E., Danovaro, R., and Dell'Anno, A.: The dark portion of the Mediterranean Sea is a bioreactor of organic matter cycling, Global Biogeochem. Cycles, 26, GB2017, https://doi.org/10.1029/2011GB004168, 2012.

Malanotte-Rizzoli, P., Artale, V., Borzelli-Eusebi, G. L., Brenner, S., Crise, A., Gacic, M., Kress, N., Marullo, S., Ribera d'Alcalà, M., Sofianos, S., Tanhua, T., Theocharis, A., Alvarez,

M., Ashkenazy, Y., Bergamasco, A., Cardin, V., Carniel, S., Civitarese, G., D'Ortenzio, F., Font, J., Garcia-Ladona, E., Garcia-Lafuente, J. M., Gogou, A., Gregoire, M., Hainbucher, D., Kontoyannis, H., Kovacevic, V., Kraskapoulou, E., Kroskos, G., Incarbona, A., Mazzocchi, M. G., Orlic, M., Ozsoy, E., Pascual, A., Poulain, P.-M., Roether, W., Rubino, A., Schroeder, K., Siokou-Frangou, J., Souvermezoglou, E., Sprovieri, M., Tintoré, J., and Triantafyllou, G.: Physical forcing and physical/biochemical variability of the Mediterranean Sea: a review of unresolved issues and directions for future research, Ocean Sci., 10, 281–322, https://doi.org/10.5194/os-10-281-2014, 2014.

Martin, J. H., and G. A. Knauer (1973), Elemental composition of plankton, Geochim. Cosmochim. Acta, 37(7), 1639– 1653.

Martin, J. H., Knauer, G. A., Karl, D. M., and Broenkow, W. W.: VERTEX: carbon cycling in the northeast Pacific, Deep-Sea Res., 34, 267–285, http://dx.doi.org/10.1016/0198-0149(87)90086-0, 1987.

Monnin, C. and Cividini, D.: The saturation state of the world's ocean with respect to (Ba,Sr)SO4 solid solutions, Geochim. Cosmochim. Ac., 70, 3290–3298, https://doi.org/10.1016/j.gca.2006.04.002, 2006.

Moutin, T. and Raimbault, P.: Primary production, carbon export and nutrients availability in western and eastern Mediterranean Sea in early summer 1996 (MINOS cruise), J. Marine Syst., 33–34, 273–288, https://doi.org/10.1016/S0924-7963(02)00062-3, 2002.

Pabortsava, K., Lampitt, R. S., Benson, J., Crowe, C., McLachlan, R., Le Moigne, F. A. C., Mark Moore, C., Pebody, C., Provost, P., Rees, A. P., Tilstone, G. H., and Woodward, E. M. S.: Carbon sequestration in the deep Atlantic enhanced by Saharan dust, Nature Geoscience, 10, 189–194, https://doi.org/10.1038/ngeo2899, 2017.

Planchon, F., Cavagna, A.-J., Cardinal, D., André, L., and Dehairs, F.: Late summer particulate organic carbon export and twilight zone remineralisation in the Atlantic sector of

592 the Southern Ocean, Biogeosciences, 10, 803–820, https://doi.org/10.5194/bg-10-803-2013,
593 2013.
594 Pujo-Pay, M., Conan, P., Oriol, L., Cornet-Barthaux, V., Falco, C., Ghiglione, J.-F., Goyet,
595 C., Moutin, T., and Prieur, L.: Integrated survey of elemental stoichiometry (C, N, P) from the
596 western to eastern Mediterranean Sea, Biogeosciences, 8, 883–899,
597 https://doi.org/10.5194/bg-8-883-2011, 2011.
598 Reygondeau, G., Guieu, C., Benedetti, F., Irisson, J.-O., Ayata, S.-D., Gasparini, S., and
599 Koubbi, P.: Biogeochemical regions of the Mediterranean Sea: An objective multidimensional
600 and multivariate environmental approach, Prog. Oceanogr., 151, 138–148,
601 http://dx.doi.org/10.1016/j.pocean.2016.11.001, 2017.
602 Sanchez-Vidal, A., Collier, R. W., Calafat, A., Fabres, J., and Canals, M.: Particulate barium
603 fluxes on the continental margin: a study from the Alboran Sea (Western Mediterranean),
604 Mar. Chem., 93, 105–117, https://doi.org/10.1016/j.marchem.2004.07.004, 2005.
605 Santinelli, C., Nannicini, L., and Seritti, A.: DOC dynamics in the meso and bathypelagic
606 layers of the Mediterranean Sea, Deep-Sea Res. Pt. II, 57, 1446–1459,
607 https://doi.org/10.1016/j.dsr2.2010.02.014, 2010.
608 Schlitzer, R.: Ocean Data View, GEO/ODV, available at: http://www.awi-bremerhaven.de/
609 (last access: 2 March 2021), 2002.
610 Simon, M. and Azam, F.: Protein content and protein synthesis rates of planktonic marine
611 bacteria, Mar. Ecol. Prog. Ser., 51, 201–213, 1989.
612 Stabholz, M., Durrieu de Madron, X., Canals, M., Khripounoff, A., Taupier-Letage, I., Testor,
613 P., Heussner, S., Kerhervé, P., Delsaut, N., Houpert, L., Lastras, G., and Dennielou, B.:
614 Impact of open-ocean convection on particle fluxes and sediment dynamics in the deep
615 margin of the Gulf of Lions, Biogeosciences, 10, 1097–1116, https://doi.org/10.5194/bg-10-
616 1097-2013, 2013.

Stange, P., Bach, L. T., Le Moigne, F. A. C., Taucher, J., Boxhammer, T., and Riebesell, U.: Quantifying the time lag between organic matter production and export in the surface ocean: Implications for estimates of export efficiency, Geophys. Res. Lett., 44, 268–276, https://doi.org/10.1002/2016GL070875, 2017.

Sternberg, E., Jeandel, C., Miquel, J.-C., Gasser, B., Souhaut, M., Arraes-Mescoff, R., and Francois, R.: Particulate barium fluxes and export production in the northwestern Mediterranean, Mar. Chem., 105, 281–295, https://doi.org/10.1016/j.marchem.2007.03.003, 2007.

Sternberg, E., Jeandel, C., Robin, E., and Souhaut, M.: Seasonal cycle of suspended barite in the mediterranean sea, Geochim. Cosmochim. Ac., 72, 4020–4034, https://doi.org/10.1016/j.gca.2008.05.043, 2008.

Stroobants, N., Dehairs, F., Goeyens, L., Vanderheijden, N., and Van Grieken, R.: Barite formation in the Southern Ocean water column, Mar. Chem., 35, 411–421, https://doi.org/10.1016/S0304-4203(09)90033-0, 1991.

Tamburini, C., Garcin, J., Ragot, M., and Bianchi, A.: Biopolymer hydrolysis and bacterial production under ambient hydrostatic pressure through a 2000m water column in the NW Mediterranean, Deep-Sea Res. Pt. I, 49, 2109–2123, https://doi.org/10.1016/S0967-0645(02)00030-9, 2002.

Tamburini, C., Boutrif, M., Garel, M., Colwell, R. R., and Deming, J. W.: Prokaryotic responses to hydrostatic pressure in the ocean – a review, Environ. Microbiol., 15, 1262–1274, https://doi.org/10.1111/1462-2920.12084, 2013.

Tanhua, T., Hainbucher, D., Cardin, V., Álvarez, M., Civitarese, G., McNichol, A. P., and Key, R. M.: Repeat hydrography in the Mediterranean Sea, data from the <i>Meteor</i> cruise 84/3 in 2011, Earth Syst. Sci. Data, 5, 289–294, https://doi.org/10.5194/essd-5-289-2013, 2013a.

Tanhua, T., Hainbucher, D., Schroeder, K., Cardin, V., Álvarez, M., and Civitarese, G.: The Mediterranean Sea system: a review and an introduction to the special issue, Ocean Sci., 9, 789–803, https://doi.org/10.5194/os-9-789-2013, 2013b.

Taylor, S. R. and McLennan, S. M.: The continental crust: its composition and evolution, Blackwell Scientific Publications, USA, 312 pp., 1985.

Van Wambeke, F., Taillandier, V., Deboeufs, K., Pulido-Villena, E., Dinasquet, J., Engel, A., Marañón, E., Ridame, C., and Guieu, C.: Influence of atmospheric deposition on biogeochemical cycles in an oligotrophic ocean system, Biogeosciences, 2020, 1–51, https://doi.org/10.5194/bg-2020-411, 2020.

670 Figure 1

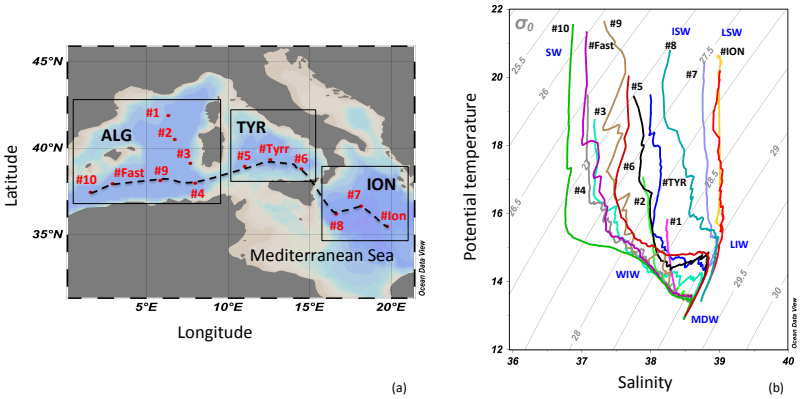

671

672

673

674

675

676 Figure 2

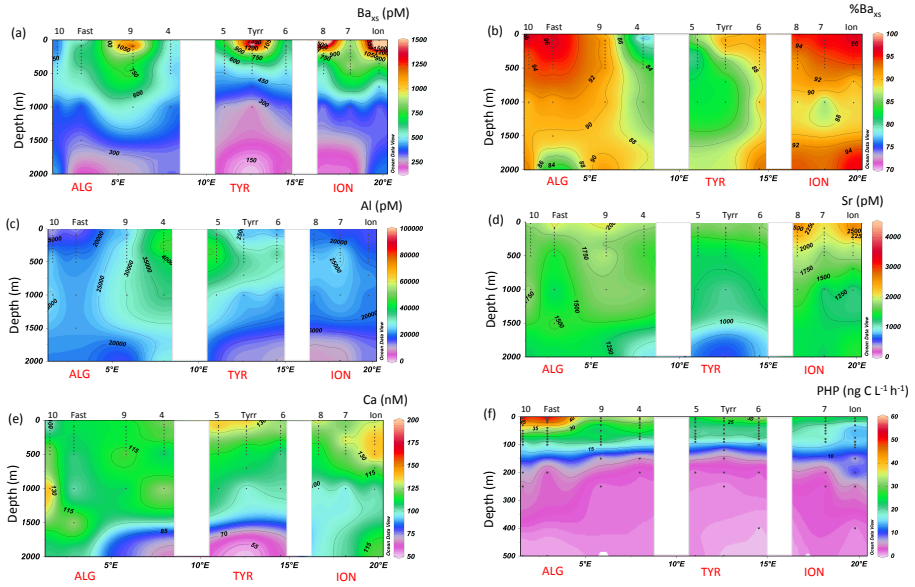

677

678

679

680 Figure 3

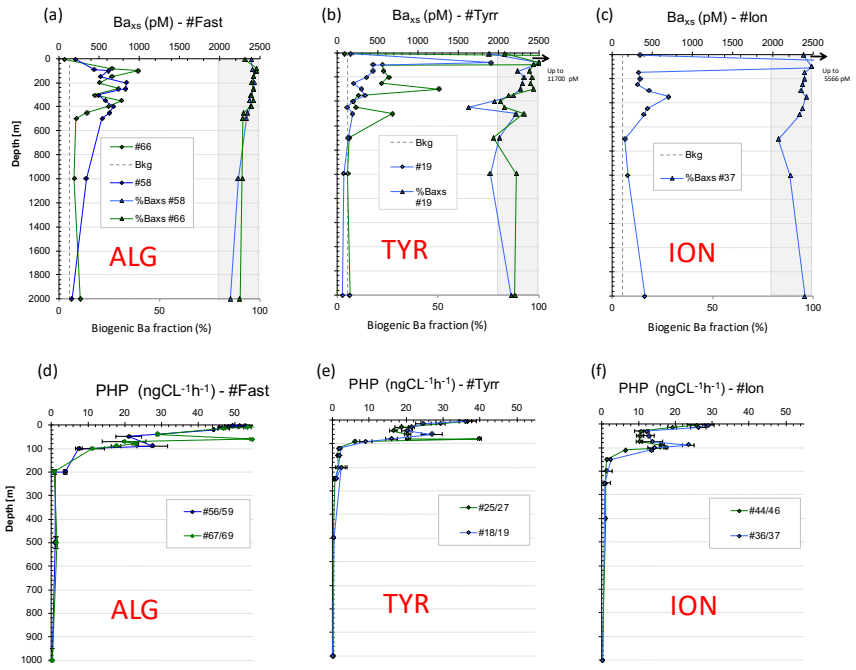

681

682

683

684 Figure 4

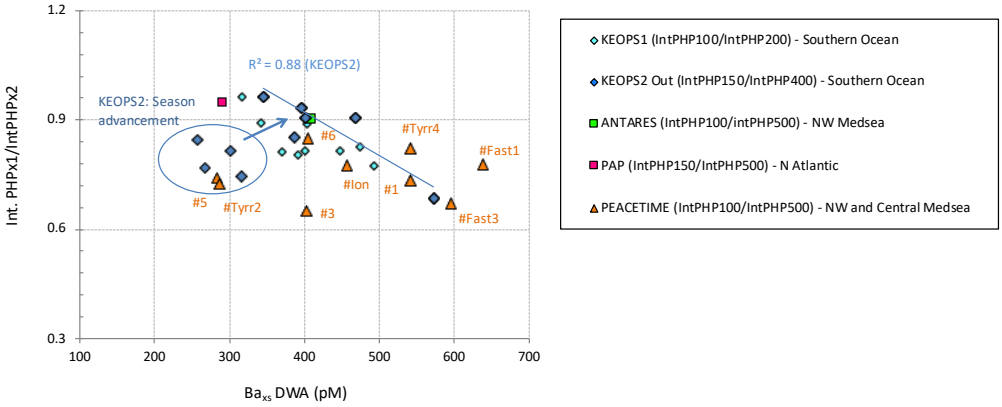

685

686

687

688

689 Figure 5

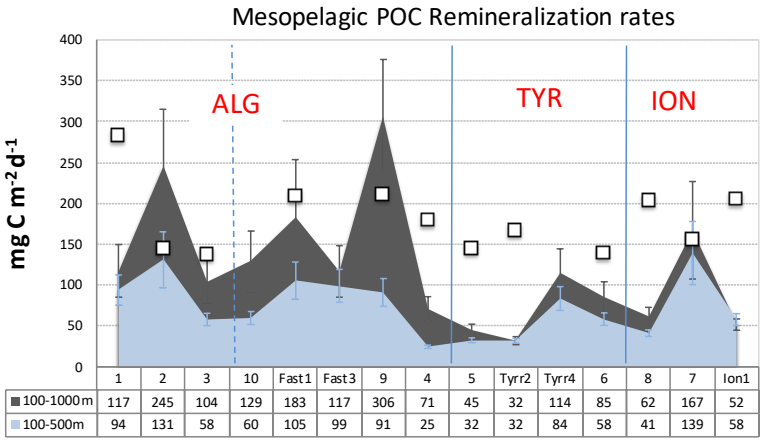

690

691

692

693 Table 1

Basin	Station #	Mesopelagic layer	DWA Ba_{xs} [pM]	MR [mg C m^{-2} d^{-1}]	MR Stnd error [%]
Algero-Provençal	1	upper	542	94	20
	1	entire	374	117	27
	2	upper	717	131	26
	2	entire	645	245	28
	3	upper	402	58	13
	3	entire	353	104	25
	4	upper	243	25	8
	4	entire	281	71	20
	9	upper	981	91	19
	9	entire	979	306	23
	Fast1	upper	638	105	21
	Fast1	entire	527	183	38
	Fast3	upper	596	99	20
	Fast3	entire	381	117	27
	10	upper	418	60	13
	10	entire	410	129	29
Tyrrhenian	5	upper	283	32	9
	5	entire	226	45	17
	Tyrr2	upper	284	32	9
	Tyrr2	entire	200	32	15
	Tyrr4	upper	542	84	17
	Tyrr4	entire	380	114	26
	6	upper	404	58	13
	6	entire	313	85	22
Ionian	7	upper	769	139	28
	7	entire	485	167	36
	ION	upper	456	58	13
	ION	entire	315	52	13
	8	upper	363	41	10
	8	entire	273	62	18

694